

New Developments of Hydroforming in China

Shijian Yuan, Zhubin He and Gang Liu

School of Materials Science and Engineering, Harbin Institute of Technology, Harbin 150001, P. R. China

This paper reviews the recent developments of hydroforming technology in China. Limited corner radius, ring hoop tension test and tube bulging test were introduced on fundamentals of hydroforming. New hydroforming and hydro-bending process of ultra-thin tubes were investigated. Ultra-thin Y-shaped parts and complex section components were manufactured and applied in aerospace and aviation industry. Applications of tube hydroforming in automotive industry in China are also presented, including the hydroforming machines and production lines, typical automotive parts and potential market. New sheet hydroforming process with controllable radial pressure was proposed to increase the formability of sheets metals. Warm tube and sheet hydroforming were analyzed and discussed. [doi:10.2320/matertrans.MF201122]

(Received August 22, 2011; Accepted December 14, 2011; Published February 1, 2012)

Keywords: tube hydroforming, sheet hydroforming, warm hydroforming, automotive, aerospace

1. Introduction

As an advanced method to manufacture lightweight components, tube hydroforming has been used in different fields, such as automotive, aeronautic and aerospace industries. In the past decades, applications of hydroformed automotive structural parts have grown to considerable scale in North American and Europe.^{1,2)} In Asia, applications of tube hydroforming in automotive industry are growing rapidly in Japan and Korea.^{3,4)} There is also a large potential market in China.^{5,6)}

In China, comprehensive and systematic research and development has been conducted on fundamental, process, die and press since 1999. As the first R&D center of tube hydroforming in China, the Engineering Research Center of Hydroforming (ERCH) from Harbin Institute of Technology (HIT) has established its leader position in this field in China. Many parts are successfully made for rockets and airplanes. Instrument panel beams developed by HIT are massively used in the car Chrysler 300, which is the first one that self-developed by HIT. Moreover, chassis part, exhaust parts, Y-shaped tubes have been applied in industry and the biggest tube hydroforming press with closing force 55000 kN was developed by HIT in the year of 2010.⁷⁻¹⁰⁾ A 50000 kN hydroforming press made by Schuler was installed in Baosteel to develop hydroforming process of automotive parts. Besides, other universities have made fundamental experiments and simulation only in lab.¹¹⁾

Sheet hydroforming or hydro-mechanical deep drawing has also found wide applications in the field of automobile and aerospace industry. Compared with conventional sheet metal deep drawing, improved forming limit, enhanced surface quality and reduced tool cost can be realized. Up to now, more than hundred types of workpieces have been manufactured in Sweden, Japan and Germany.¹²⁾ In China, new processes have been proposed to improve the formability of aluminum alloys.^{13,14)} The biggest sheet hydroforming press with 13500 kN closing force was developed by HIT and successful applications have been realized in aerospace and aviation industries.¹⁵⁾

In this paper, the latest developments of hydroforming in China will be introduced. New research results in funda-

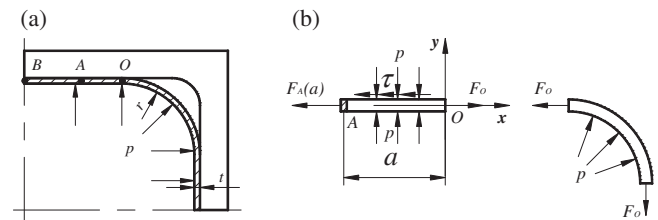


Fig. 1 Force analysis of corner filling process. (a) Shape of corner (b) force analysis.

mentals, innovative process and typical applications in different fields will be presented and discussed.

2. Tube Hydroforming

2.1 Fundamentals of tube hydroforming

2.1.1 Limited corner radius

In calibration stage, corner radius decreases as inner pressure increases. In practice, however, the corner radius can not become smaller even though the inner pressure is still increasing.¹⁶⁾

The minimum corner radius that can be achieved before fracturing during corner filling, is called the limited corner radius r_{lim} . The strain increment at the transition point O in Fig. 1 can be written as:

$$d\epsilon_x = \frac{d\lambda p}{2t}(t + r - \mu a) \quad (1)$$

Where, t , r are the instantaneous thickness and radius at the corner, a is the length of the rectangular section, p is the inner pressure, μ is the friction coefficient between the tube and die cavity.

When $d\epsilon_x = 0$, equation for the limited corner radius can be obtained as:

$$r_{lim} = \mu a - t \quad (2)$$

The above equation shows that the limited corner radius is determined by the friction coefficient, the length of rectangular section and the tube thickness, and is no longer affected by inner pressure.

Table 1 Limited corner radius with different lubricants.

Lubricants	Limited corner radius, r_{lim}/mm
No lubricant	7.50
Oil	6.50
MoS ₂	4.65
PE film	2.30

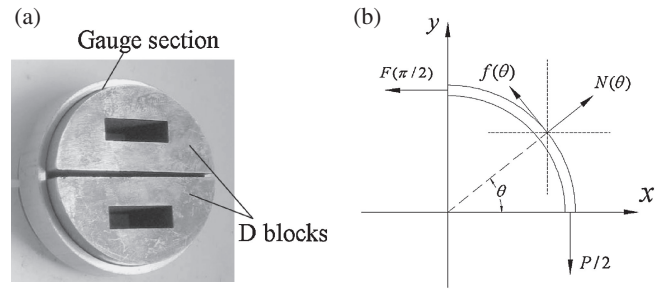


Fig. 2 Force analysis of the ring specimen in hoop tension test. (a) Ring specimen and D-blocks (b) force analysis of ring specimen.

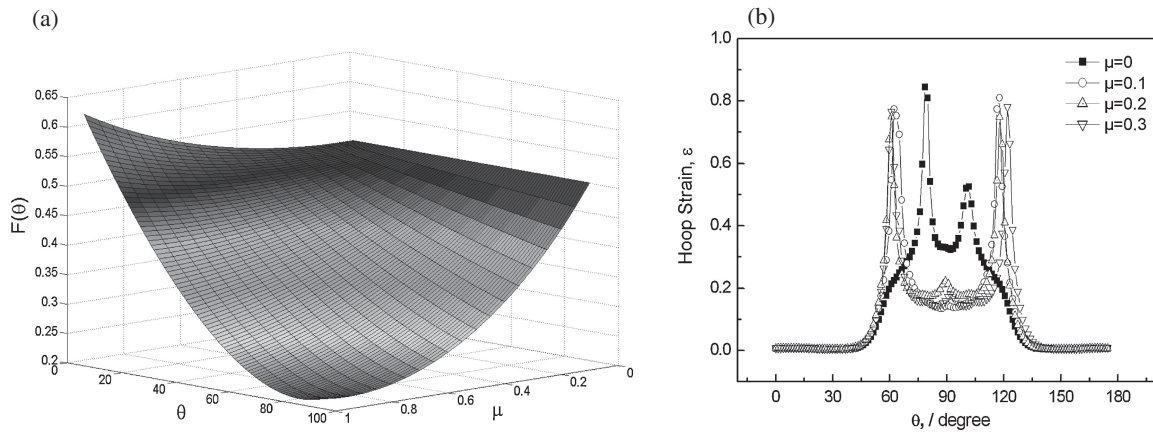


Fig. 3 Effect of friction on the hoop tension force and hoop strain distribution. (a) Hoop tension force distribution (b) hoop strain distribution.

The limited corner radius at different lubrication conditions was measured by an experiment as given in Table 1. It can be seen that as lubrication condition was improved, better corner filling can be realized and smaller corner radius can be achieved.

2.1.2 Effect of friction in ring hoop tension test

Ring Hoop Tension Test (RH TT) is a new method proposed to give a better evaluation of the formability along hoop direction of a tube. Universal tensile testing machine is used to expand a ring specimen directly with a special test fixture. When the ring specimen was expanded, its original ring shape can be maintained, which can avoid the effect of work hardening during traditional flat specimen preparation, especially for tube with small radius or tube with poor formability.

The effect of the friction between specimen and D-blocks was investigated.^{17,18)} The force analysis model is given in Fig. 2. A formula to calculate the hoop tension force is given as:

$$F(\theta) = \frac{Pm}{\sin \theta [\mu(\pi - 2) + 2]} + \frac{1}{\sin \theta} \left[\sin \theta - \mu(1 - \cos \theta) - \frac{2(\mu + 1)m}{\mu(\pi - 2) + 2} \right] \times \frac{\mu(\pi - 2) + 4}{2(\pi - 2)\mu(1 - \mu) + 8} \cdot P \quad (3)$$

Where: $m = (\theta \sin \theta + \cos \theta - 1) + \mu(\theta \cos \theta - \sin \theta)$, $N(\theta)$, $F(\theta)$ and $f(\theta)$ are the radial force, hoop force and friction force, respectively.

The distribution of hoop force is given in Fig. 3, together with the hoop strain distribution obtained by numerical simulation. It can be seen that uniform distribution of hoop force can be realized when $\mu = 0$. That means the specimen will deform homogeneously. As the friction coefficient increases, the hoop tension force on the top position will be decreased significantly and deformation will mainly occur on two sides. Maximum hoop strain can also be seen on both sides of the specimen, as shown in Fig. 3(b).

2.1.3 Relationship between thickness and bulging height in tube bulge test

Accurate determination of tube mechanical properties is not only the base for tube choosing and process planning, but also the preconditions of finite element (FE) simulations for tube hydroforming process. Tube bulge test is a direct method to determine the mechanical properties of tubular materials. In order to obtain relationship between effective stress and effective strain of tube, the pole thickness during tube bulge test is required. However, it is difficult to measure the pole thickness during bulging test in practice.

Figure 4 shows the analytical model for tube bulge test, assuming the profile of the bulging zone can be described by ellipsoid surface.¹⁹⁾

For tested tube with two fixed ends and free ends, the thickness at the middle pole t_p can be given respectively as below:

$$t_p = t_0 \left(1 + \frac{h}{R_0} \right)^{-1 - \frac{1}{3\alpha^2 - 2}} \quad (4)$$

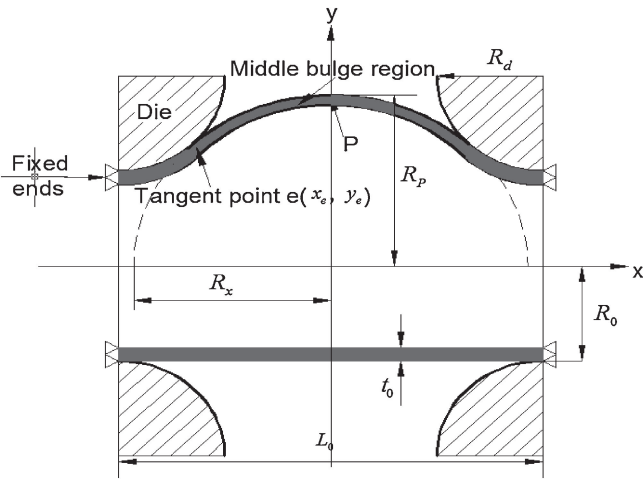


Fig. 4 Analytical model of tube bulge test.

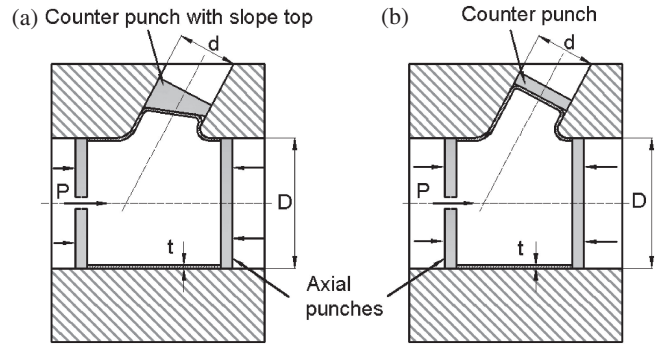


Fig. 6 Schematic of two step hydroforming. (a) Preforming (b) final forming.

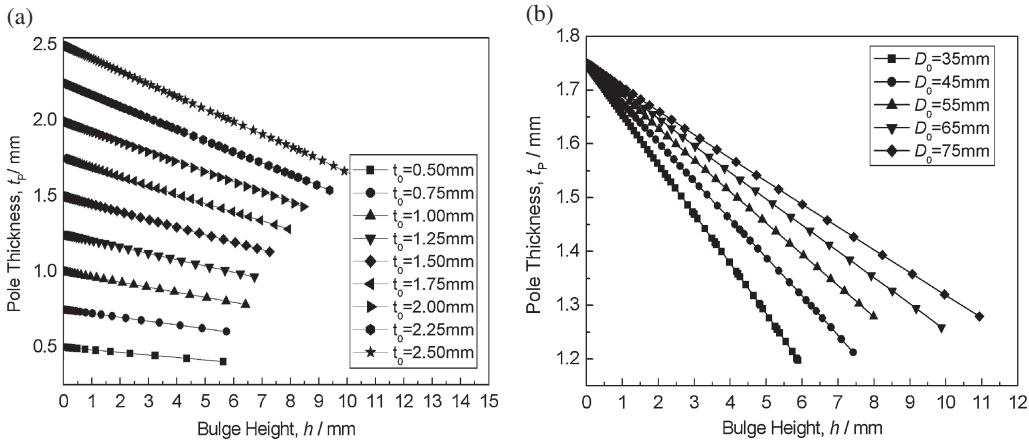


Fig. 5 Variation of t_p with h for tubes with different t_0 and different D_0 . (a) Effect of t_0 (b) effect of D_0 .

$$t_p = t_0 \left(1 + \frac{h}{R_0} \right)^{-1 + \frac{2R_0^2}{4R_0^2 + 6R_0h + 3h^2}} \quad (5)$$

Where $\alpha = R_z/R_p$ is the ratio of two semi-radius as shown in Fig. 4.

A linear relation between t_p and h exists, which can be expressed as:

$$t_p = t_0 - bh. \quad (6)$$

Where b is a parameter relating to material and dimensions of tube specimen, which can be determined by numerical simulation or experiment.

Figure 5 shows the change of pole thickness with different tube thickness and diameter. It is easy to find that the pole thickness will decrease almost linearly as the bulge height increases.

According to the correlation between the pole thickness and the bulge height, the measuring of the pole thickness during tube bulge test can be avoided, which will make the test method more feasible and effective in practice.

2.2 Hydroforming of ultra-thin tubes in aerospace and aviation industry

2.2.1 Hydroforming of stainless steel Y-shaped tube

Y-shaped tubes are more difficult to be formed compared

with T-shaped tubes due to its unsymmetrical shape, especially for ultra-thin tube with protrusion of small radius. The forming of a Y-shaped stainless steel tube with $D/t = 183$ (ratio of diameter to thickness) and $d/D = 0.45$ (ratio of protrusion diameter to main tube) was investigated. The diameter of the tube and protrusion is 220 and 100 mm, the tube thickness is 1.2 mm.

Counter punch is usually used to prevent the over-thinning and early fracture at the protrusion position. However, if a straight counter punch is used, a free bulging at the protrusion will occur at the beginning. That means in this period, the counter punch does not work. To improve the thickness distribution, a counter punch with a slope top as shown in Fig. 6 was designed to change the stress state at the top of the protrusion.²⁰⁾

In preforming stage, the protrusion will be constrained by the counter punch with a slope top, and free bulging is avoided at the initial stage. The stresses state and deformation situation are improved and the local thinning at the top of the protrusion is lowered.

Figure 7(a) shows the defects by one step hydroforming. Cracking occurred at the protrusion tip and wrinkling appeared in the bottom area of the main tube. It is difficult to avoid both the wrinkling and cracking by using one step hydroforming process.

By using the two step hydroforming, Y-shaped tube was produced successfully. Figure 7(b) shows the part after preform. Figure 7(c) shows the sound part after final forming, both wrinkling and cracking defects were avoided.

2.2.2 Hydroforming of aluminum alloy Y-shaped tube

A kind of 5000 series aluminum alloy tube is used to form a Y-shaped tube with $D/t = 40$. Optimized loading path was obtained by simulation, and a sound component was produced as shown in Fig. 8. On the formed part, thinning occurs mainly at the protrusion top, and thickening occurs at the main tube.²¹⁾ There is a thickness invariable line between the thinning and the thickening regions, which are V-shaped and located in the lower half of the branch, as shown in Fig. 8(b), respectively.

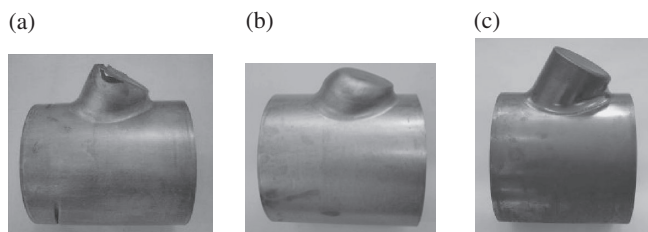


Fig. 7 Experimental results of Y-shaped tube. (a) Wrinkle and crack (b) preform (c) final form.

2.2.3 Hydroforming of ultra-thin component with complex sections

Figure 9 shows the hydroformed integral stainless steel inlet.²²⁾ It is a thin-walled component with curved axis and complex polygonal-sections. Eight stamped pieces are needed to make the inlet by conventional stamping and welding process. It is very difficult to control the deformation during welding. The integral part is successfully hydroformed by using the tube with 200mm diameter and 0.5 mm thickness. The maximum thinning of the hydroformed part is 18.2% and the thickness and the corner radius are corresponding with the design requirements.

2.3 Hydro-bending of ultra-thin tube

Figure 10 illustrates the principle of the hydro-bending process of double-layered tube.²³⁾ The inner tube, i.e. ultra thin-walled tube to be obtained, is wrapped with a mild steel outer thicker tube, which is a temporary assistant and will be removed after hydro-bending. Then the double layered tube is sealed at the two ends with end caps and pre-pressurized by a pump to a desired value as supporting internal pressure [Fig. 10(a)]. Then the double layered tube is bent as the upper die moves down [Fig. 10(b)]. After bending, the outer layer tube is cut into two halves along the neutral plane and separated from the inner tube [Fig. 10(c)]. Finally, the ultra thin-walled elbow tube can be obtained.

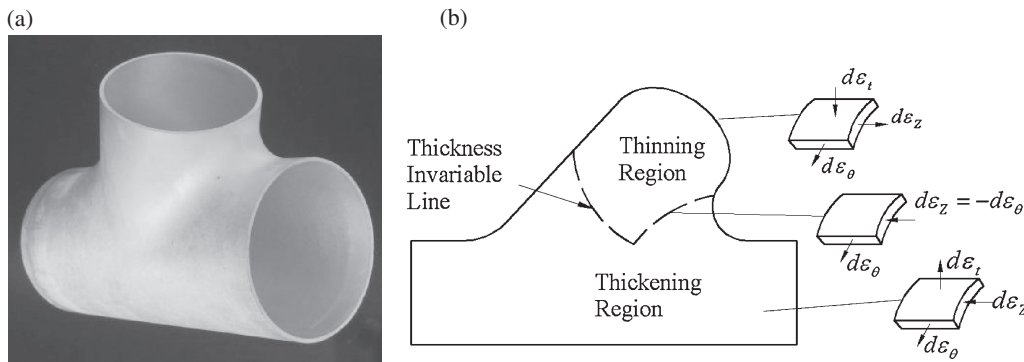


Fig. 8 Thickness distribution, thickness invariable line and strain states in different regions. (a) Formed part (b) thickness invariable line.

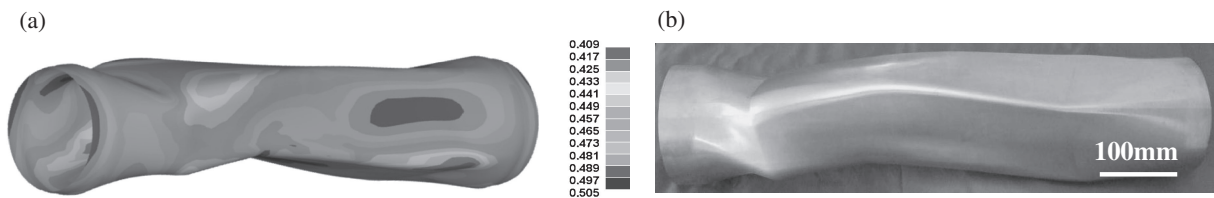


Fig. 9 Integral stainless steel inlet. (a) Thickness distribution (mm) (b) hydroformed part.

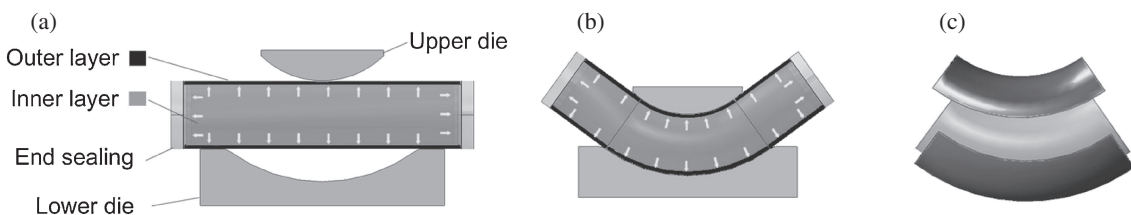


Fig. 10 Principle of the hydro-bending process of double-layered tube. (a) Pre-filling and pressurized (b) hydro-bending (c) removing of outer tube.

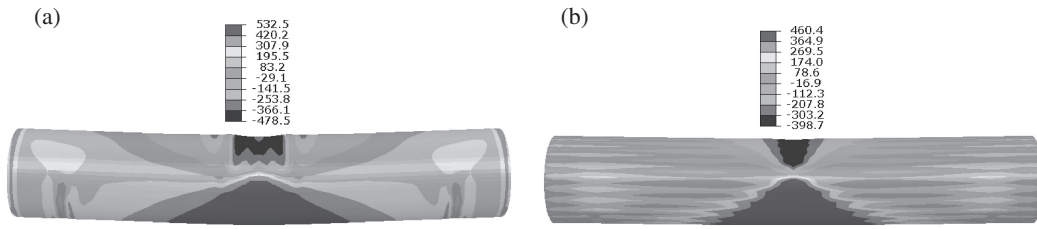


Fig. 11 Axial stress (MPa) distribution of inner tube. (a) $t_{out} = 1$ (b) $t_{out} = 10$.

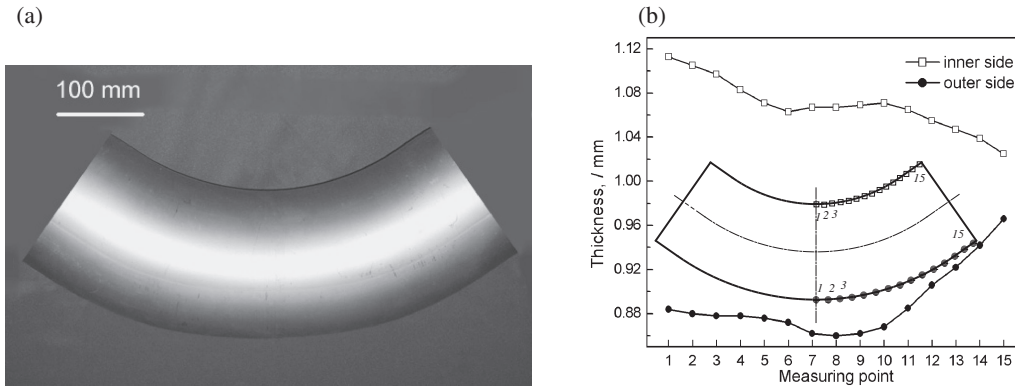


Fig. 12 Ultra thin-walled elbow with $D/t = 180$. (a) Elbow tube (b) thickness (mm) distribution.

Table 2 Hydroforming machines and production lines in China.

Manufacturer	Press tonnage (/×10 kN)	Press table size (/mm)	Typical products	Annual product	Press provider
FAW	3500	2400 × 1600	engine cradle, chassis, exhaust pipes	100,000	AP&T, Sweden
Y-Tech	3500	2600 × 2500	engine cradle	50,000	Japan
Baosteel	5000	3150 × 2150	engine cradle, chassis	150,000	Schuler, Germany
Sunda Co.	5500	5000 × 2500	chassis, frames	200,000	HIT, China
Yuanlongda Co.	3000	2400 × 1600	chassis, frames	150,000	HIT, China
Jieda Co.	3000	2400 × 2000	chassis, frames	150,000	HIT, China
Huake Co.	500	1400 × 900	exhaust pipes	100,000	HIT, China
Benma Tech. Co	630	1800 × 1200	chassis, frames	100,000	HIT, China
HIT	2000	2200 × 1800	Automotive, aerospace and aviation parts	R&D 50,000	HIT, China

Figure 11 shows the axial stress distribution of inner tube after hydro-bending, using outer tube of different thickness t_{out} . It can be seen that the axial compressive stress decreased as the thickness of outer tube changed from 1 to 10 mm, and wrinkling at the inside can be eliminated.

Figure 12 shows the ultra-thin elbow tube made by hydro-bending process. Its diameter (D) is 180 mm, thickness (t) 1 mm, i.e., the diameter-to-thickness ratio $D/t = 180$. The thickness distribution along axial direction is also given. The maximum thinning ratio at outside is 14% and the maximum value of non-circularity is only 3%.

2.4 Application of tube hydroforming in automotive industry

2.4.1 Hydroforming machines and production lines in China

In the year 2010, 18 million automobiles were produced and sold in China. It was predicted by China SAE that 10

million hydroformed automotive parts will be needed in next 3–5 year in China and 30–50 hydroforming production lines will be installed. Automotive parts produced by these lines will be used instead of the parts imported abroad and for the cars developed by Chinese companies. However, there are only about ten hydroforming machines in China today, as shown in Table 2 (also see Fig. 13), which can not meet the demand of products from automotive industry.

2.4.2 Typical automotive parts

Figure 14 shows an engine cradle developed by HIT for BESTURN car of FAW, China. The engine cradle has a 3D axis and 18 typical cross-sections varying from rectangular, trapezoidal to irregular. Several reasonable petal-like shape preforms have been designed for these typical cross-sections, by which the calibration pressure was reduced and the thickness distribution was more uniform. Mass production is realized in 2011, and 400 pieces can be produced every day.²²⁾

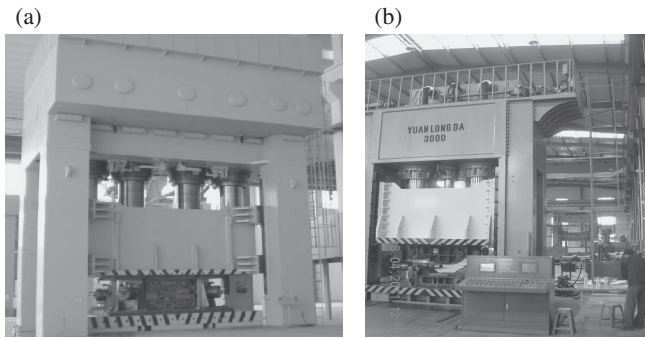


Fig. 13 Hydroforming presses developed by HIT used in automotive industry. (a) Closing force 55000 KN (b) closing force 30000 KN.

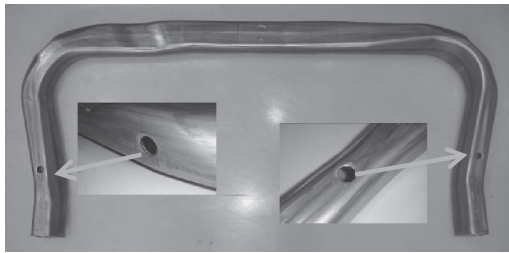


Fig. 14 Hydroformed engine cradle.



Fig. 15 Hydroformed front beam holder.



Fig. 16 Hydroformed engine cradle chassis.

Figure 15 shows the front beam holder for an SUV. It is a thin-walled component with 3D axis and rectangular cross-section. The steel of 440 MPa was used. It is successfully formed by using CNC bending, preforming and hydroforming.²²⁾

Figure 16 shows the prototype of a chassis part, which is with 3D axis and several typical cross-sections varying from rectangular, trapezoidal to irregular. The material of 440 MPa was used. The biggest difficulty to form this part is that there is a small bending radius, which can not be formed from a tube by conventional bending process.²²⁾

Figure 17 shows the hydroformed torsion beam which is hollow component with V-type cross-section. It is successfully formed by using the U-type preform.²²⁾

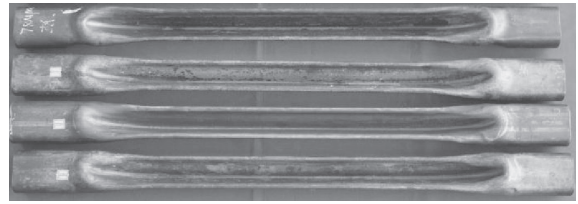


Fig. 17 Hydroformed torsion beam.

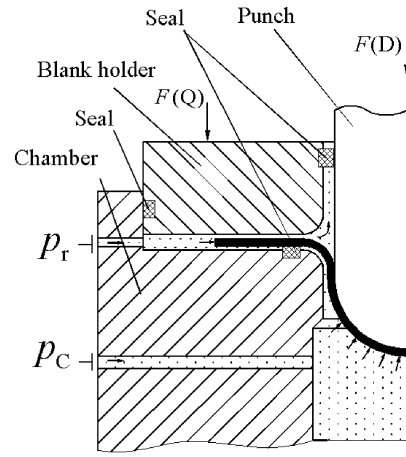


Fig. 18 Hydroforming with controllable radial pressure.

3. Sheet Hydroforming with Controllable Radial Pressure

The sheet hydroforming with controllable radial pressure is shown in Fig. 18. Based on conventional hydroforming, a controllable radial pressure P_r is imposed to the rim of flange besides the chamber pressure P_c . Because sealing rings exist, the radial pressure P_r and the chamber pressure P_c can be loaded and controlled independently. The loaded radial pressure can be larger than the chamber pressure. Thus, the radial pressure P_r aids to push the flange to flow into the chamber when the punch penetrates into the chamber. At the same time, the dual fluid lubrication can be generated and decrease the friction between the flange and the blank holder, or between the flange and the die. Therefore, serious thinning can be eliminated and forming limit can be improved.²⁴⁾

Figure 19 shows the relation between limited drawing ratio (LDR) and radial pressure. It can be seen that $LDR = 2.4$ can be reached when the radial pressure is 5 MPa, and $LDR = 2.8$ can be achieved when radial pressure is 40 MPa. LDR is improved because the stress state of the material in flange zone is changed essentially by additional radial pressure.^{25,26)}

4. Warm Hydroforming

4.1 Formability evaluation of AZ31B tube in warm forming

To evaluate the formability of AZ31B extruded tube, bulging test was carried out at different temperatures from R.T. up to 480°C. Bursting pressure and maximum expansion ratio (MER) of the tube were obtained, as shown in Fig. 20.

The fracture surface after bursting was analyzed and compared with that by tensile test along axial direction.²⁷⁾ The MER value remain almost unchanged from R.T. to 100°C. In the temperature interval between 100 and 480°C, an *oblique N model* can be used to describe the variation of MER value. The first peak and the bottom MER value occurred at 160 and 330°C, respectively, and about 30% expansion ratio was reached at 480°C. The bursting pressure decreased almost linearly as testing temperature increased. The fracture mode changed from inter crystalline fracture to gliding fracture. However, burnt structure appeared when the forming temperature was about 480°C.

4.2 Warm hydroforming of tube with large expansion ratio

When formed at elevated temperature, the effect of work-hardening decreases and material softening can be observed from the stress–strain curve by tension test, especially at high temperature. In addition, the diameter in the bulging zone will increase and thickness will decrease. That means, deformation will be focused in the zone where bulging happen first, and no homogeneous deformation can be realized and early fracture will happen.

In order to increase the formability of tube at elevated temperature, deformation position and sequence should be controlled. Figure 21 shows the Al6061 part with large

expansion ratio formed by hot metal gas forming (HMGF) with local constraint.²⁸⁾ The middle zone of the tube was constrained in the first stage, and a preformed specimen was formed. In the last stage, constraints were removed and the final part was successfully formed. The maximum expansion ratio is about 92%.

4.3 Formability evaluation of 5A02 sheet in warm hydroforming

Experiments on warm sheet hydroforming were conducted to evaluate the formability of 5A02 sheet in forming of round cup. The effect of forming temperature, duration time and forming pressure were investigated.²⁸⁾ Figure 22 shows the profile and corner radius of the formed part at different conditions. The unchanged parameters are given in the bracket.

It can be seen that in the forming of round cup, temperature, duration time and forming pressure are three main factors that determine the results of warm sheet hydroforming process. In order to reduce the duration time, higher forming pressure can be used. However, enough duration time about 60 s are usually needed, especially when formed with relatively low temperature.

Warm sheet hydroforming press has been developed in Beihang University. Heated oil is used as pressure media. The maximum liquid pressure is 100 MPa. The forming press is with 6300 kN main cylinder and 2500 kN binder cylinder, with variable bank-holding force control.

Effect of forming temperature on the formability of typical aluminum alloy sheet was investigated²²⁾. Figure 23(a) shows the hydroformed cups at different temperatures. The maximum drawing height or the LDR increased obviously as temperature increased. Part in aircraft industry as shown in

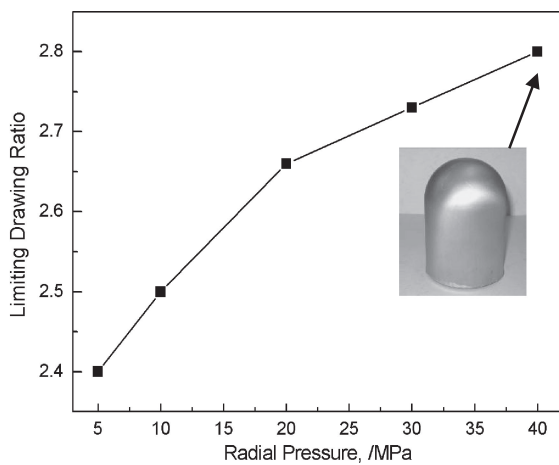


Fig. 19 LDR with different radial pressures.

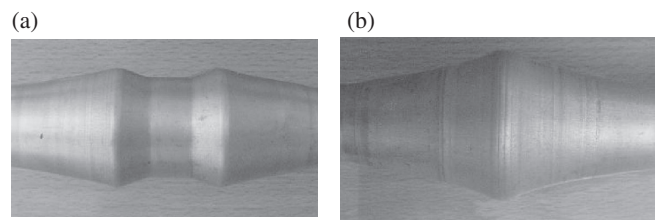


Fig. 21 Formed tubular part with large expansion ratio by local constraint.²⁸⁾ (a) Preformed specimen (b) final part.

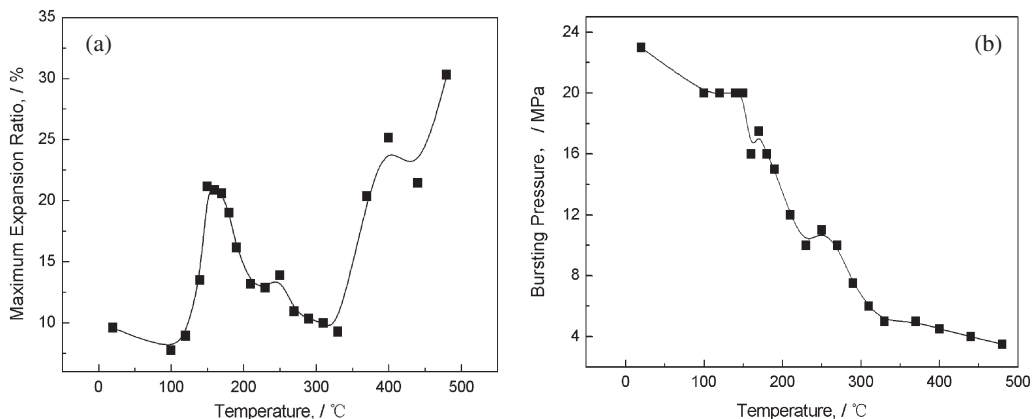


Fig. 20 Maximum expansion ratio and bursting pressure at different temperatures.²⁷⁾ (a) Maximum expansion ratio (b) bursting pressure.

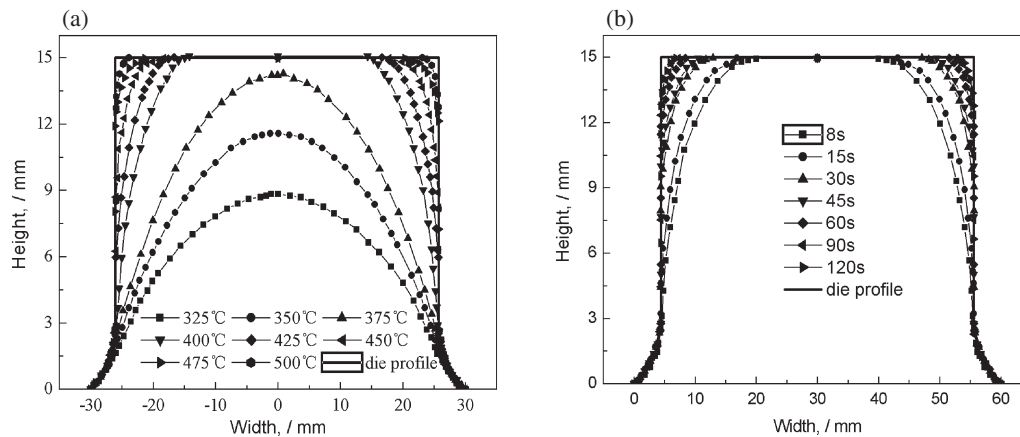


Fig. 22 Profile and corner radius of the formed round cup.²⁸⁾ (a) Temperature (2.5 MPa, 30 s) (b) duration time (450°C, 2.5 MPa).



Fig. 23 Warm hydroformed part with heated oil. (a) Cups with different temperature (b) aluminum part.

Fig. 23(b) was formed on the warm hydroforming press. The material is 2B06-M, which has very poor formability at room temperature. The part is with conical side wall and curved flange. Many positions are unsupported in forming process and deformation is extraordinary non-uniform.

5. Conclusions

In the past several years, important developments in both tube hydroforming and sheet hydroforming have been achieved in China.

In tube hydroforming, progresses in the fundamentals have been obtained. In automotive industry, more and more hydroformed components have been manufactured in large volume production. The biggest capacity of hydroforming machines developed by HIT is 55000 KN and more hydroforming production lines will be installed in China to meet the requirement from industry. Moreover, applications of hydroforming are extended from automotive industry to aerospace and aviation industry. For applications in aerospace and aviation industry, the diameter of tubes is larger and thickness is thinner.

In sheet hydroforming, new methods have been proposed and investigated in order to improve the formability of aluminum alloys. Complex shape components with poor formability materials can be formed using these special methods.

Warm hydroforming or forming at elevated temperature is another approach to improve the formability of tube and sheet metals. Heated oil can be used as pressure medium when formed at temperature lower than 300°C.

Acknowledgements

This study was financially supported by the National Natural Science Found for Distinguished Young Scholars (No. 50525516) and the National Natural Science Foundation of China (Nos. 59975021, 50375036). The authors would like to take this opportunity to express their sincere appreciations.

REFERENCES

- 1) K. P. Hennig: Proc. 3rd Int. Conf. on Tube Hydroforming, ed. by S. J. Yuan, (The H.I.T Press, Harbin, 2007) pp. 11–18.
- 2) M. Liewald: Proc. 3rd Int. Conf. on Tube Hydroforming, ed. by S. J. Yuan, (The H.I.T Press, Harbin, 2007) pp. 19–26.
- 3) S. Fuchizawa: Proc. 3rd Int. Conf. on Tube Hydroforming, ed. by S. J. Yuan, (The H.I.T Press, Harbin, 2007) pp. 1–10.
- 4) K. J. Kim, J. S. Kim, B. I. Choi, K. H. Kim, H. H. Choi, C. W. Kim, G. K. W. Kang, J. H. Song and C. W. Sung: *J. Mech. Sci. Technol.* **21** (2007) 1523–1527.
- 5) S. J. Yuan, G. Liu and X. S. Wang: Proc. 3rd Int. Conf. on Tube Hydroforming, ed. by S. J. Yuan, (The H.I.T Press, Harbin, 2007) pp. 27–38.
- 6) S. J. Yuan, G. Liu, Z. B. He, X. S. Wang, B. G. Teng and Y. C. Xu: *Digital Manufacture Science* **6** (2008) 1–34 (in Chinese).
- 7) S. J. Yuan, C. Han and X. S. Wang: *Int. J. Mach. Tools Manuf.* **46** (2006) 1201–1206.
- 8) G. Liu, S. J. Yuan and B. G. Teng: *J. Mater. Process. Technol.* **177** (2006) 688–691.
- 9) C. Han and S. J. Yuan: *Adv. Mater. Res.* **44–46** (2008) 143–150.
- 10) S. J. Yuan and G. Liu: Proc. 4th Int. Conf. on Tube Hydroforming, ed. by Y. M. Hwang (National Sun Yat-sen University Press, Taiwan, 2009) pp. 13–24.
- 11) X. H. Xu, S. H. Li, W. G. Zhang and Z. Q. Lin: *J. Mater. Process. Technol.* **209** (2009) 158–164.
- 12) H. Amino, K. Makita and T. Maki: Proc. of Int. Conf. on New Developments in Sheet Forming Technol. Stuttgart-Germany: Fellbach, (2000) pp. 39–66.
- 13) Y. Chen and Y. C. Xu: *J. Mater. Sci. Technol.* **12** (2004) 406–408 (in Chinese).
- 14) S. H. Zhang, L. H. Lang, D. C. Kang, J. Dankert and K. B. Nielsen: *Int. J. Mach. Tools Manuf.* **40** (2000) 1492–1497.
- 15) L. H. Lang and Z. R. Wang: *J. Mater. Process. Technol.* **151** (2004) 165–177.
- 16) P. Song, X. S. Wang, C. Han, Y. C. Xu and S. J. Yuan: *J. Mech. Eng.* **46** (2010) 59–64.
- 17) Z. B. He, S. J. Yuan, W. W. Cha and Y. C. Liang: *Acta Metall. Sinica* **44** (2008) 423–427.
- 18) Z. B. He, S. J. Yuan, G. Liu, J. Wu and W. W. Cha: *J. Mater. Process.*

- Technol. **210** (2010) 877–884.
- 19) Y. L. Lin, Z. B. He and S. J. Yuan: *Acta Metall. Sinica* **46** (2010) 729–735.
- 20) G. Liu, J. Y. Peng, X. S. Wang, S. Q. Zhu and S. J. Yuan: *Adv. Mater. Res.* **189–193** (2011) 2796–2800.
- 21) G. Liu, J. Y. Peng, G. N. Chu, S. Q. Zhu, H. T. Xiao and S. J. Yuan: *Steel Res. Int.* **81** (2010) 536–539.
- 22) S. Yuan, Z. He and G. Liu: Proc. 5th Int. Conf. on Tube Hydroforming TUBEHYDRO2011, (2011) pp. 2–13.
- 23) B. G. Teng, L. Hu and S. J. Yuan: Proc. 6th Int. Conf. on Physical and Numerical Simulation of Materials Processing, ed. by J. T. Niu, China, (2010) p. 77.
- 24) Y. C. Xu, X. Liu, X. J. Liu and S. J. Yuan: *J. Cent. South. Univ. Technol.* **16** (2009) 887–891.
- 25) Y. C. Xu, X. Liu, S. J. Yuan and D. C. Kang: *Steel Res. Int.* **81** (2010) 632–635.
- 26) Y. C. Xu, F. Li, X. Liu and S. J. Yuan: *J. Miner. Metal. Mater. Soc.* **63** (2011) 36–38.
- 27) Y. L. Lin, Z. B. He, S. J. Yuan and J. Wu: *Trans. Nonferrous Met. Soc. China* **21** (2011) (accepted).
- 28) Z. B. He, X. B. Fan, Y. C. Xu and S. J. Yuan: *Rare Metal Mater. Eng.* **40** (2011) (accepted).